Effect of Deformation Temperature on Microstructure Evolution in ARB Processed Ultralow Carbon IF Steel

AUTHOR(S):

Kamikawa, Naoya; Tsuji, Nobuhiro

CITATION:

Kamikawa, Naoya ...[et al]. Effect of Deformation Temperature on Microstructure Evolution in ARB Processed Ultralow Carbon IF Steel. Materials transactions 2011, 53(1): 30-37

ISSUE DATE:

2011-12

URL:

http://hdl.handle.net/2433/171911

Materials Transactions, Vol. 53, No. 1 (2012) pp. 30 to 37
Special Issue on Advanced Materials Science in Bulk Nanostructured Metals

Effect of Deformation Temperature on Microstructure Evolution in ARB Processed Ultralow Carbon IF Steel

Naoya Kamikawa[1,*] and Nobuhiro Tsuji[2]

[1]*Institute for Materials Research, Tohoku University, Sendai 980-8577, Japan*
[2]*Department of Materials Science and Engineering, Kyoto University, Kyoto 606-8501, Japan*

The effect of deformation temperature on the microstructure evolution was investigated in the range from room temperature to 600°C for an ultralow carbon interstitial free steel deformed to high strain by accumulative roll-bonding (ARB). In the whole temperature range, the microstructure was being subdivided by deformation-induced boundaries, and the spacing of such boundaries decreased with increasing the applied strain. The mechanism of this microstructure evolution is known as grain subdivision. In the warm-temperature ARB at 400°C and above, a quite uniform lamellar boundary structure elongated to the rolling direction was obtained after high strain, where the boundary spacing tended to be saturated above strain of approximately 4 and the saturated boundary spacing became smaller when the deformation temperature was lower. It is suggested that the microstructure after high strain deformation is determined by a balance of deformation-induced grain subdivision and restoration processes such as recovery and short-range boundary migration, and that the saturated boundary spacing is explained as a function of the Zener–Hollomon parameter. However, localized shear banding occurred at high strain in the room-temperature ARB, leading to inhomogeneities in the microstructure. It is therefore considered that a moderate deformation temperature as well strain rate has to be chosen to avoid shear localization and obtain homogeneous nanostructures. [doi:10.2320/matertrans.MD201115]

(Received July 26, 2011; Accepted September 7, 2011; Published December 25, 2011)

Keywords: *nanostructured metals, severe plastic deformation (SPD), interstitial free (IF) steel, deformation temperature, grain subdivision*

1. Introduction

Nanostructured metals with an average grain size of less than 1 μm show a very high strength, good toughness and other excellent mechanical properties,[1–5] and therefore such metals are expected to be advanced structural materials for the next generation. Many different techniques have been proposed to produce nanostructured metals,[6–9] and plastic deformation to ultrahigh strain, i.e. severe plastic deformation (SPD),[8,9] is a promising route to produce bulk nanostructured metals with relatively large sample dimensions.

In order to establish SPD processes as a microstructure controlling technique for structural metallic materials, a formation mechanism of nanostructures during SPD has to be well understood. It has been proposed that grain refinement takes place during SPD processes in a way that original coarse grains are subdivided by deformation-induced high-angle boundaries into finer-scaled crystallites with increasing the applied strain. This mechanism has been termed *grain subdivision* by plastic deformation.[10,11] On the other hand, it has also been reported[12–15] that the average spacing of deformation-induced boundaries tends to be saturated at high strain, indicating that some restoration processes, such as recovery and boundary migration, are operating in addition to grain subdivision. However, detailed mechanism of such a structural saturation has not yet been understood. Since grain subdivision by plastic deformation is a dislocation-related process and therefore should be thermally activated, the microstructure evolution may strongly depend on the deformation temperature that can affect glide, accumulation, annihilation of dislocations, and boundary migration during the deformation.

In the present study, in order to furthermore understand the formation mechanisms of nanostructures by high strain deformation, in particular the mechanism of the structural saturation, the effect of deformation temperature on microstructure evolution is studied in an ultralow carbon interstitial free (IF) steel deformed to high strain by accumulative roll-bonding (ARB),[16,17] which is a kind of SPD process using a rolling deformation.

2. Experimental

A Ti-added IF steel (Fe–0.002 mass%C–0.003N–0.01Si–0.17Mn–0.012P–0.01Cu–0.02Ni–0.072Ti) was used in this study. The starting material had a fully recrystallized ferrite structure with an average grain size of 20 μm.

Sheets with a thickness of 1 mm, a width of 30 mm and a length of 300 mm were prepared for the ARB process. After being degreased and wire-brushed, two sheets of the starting materials were stacked and roll-bonded by approximately 50% thickness reduction in one pass. The ARB process was carried out at four different temperatures: room temperature (RT), 400°C, 500°C and 600°C. In the warm-temperature ARB at 400°C and above, the stacked sheets were held in an air furnace set at each temperature for 10 min and immediately roll-bonded. The warm-temperature ARB was carried out without any lubricant between the rolls and the sheet surfaces to enhance a structural refinement by introducing a large amount of surface shear deformation.[18,19] In the room-temperature ARB, 50% reduction in one pass, which is necessary to obtain a good bonding, cannot be achieved by the non-lubricated rolling, due to a significant elastic deformation of a rolling mill caused by a large rolling force. Therefore, a well-lubricated rolling has been carried out at room temperature, and the ARB samples with a good bonding have successfully been produced. In all cases, the rolling was carried out at a rolling speed of 17.5 m min^{-1} by a two-high mill with rolls 310 mm in diameter, corresponding to an average nominal strain rate of 19 s^{-1}. The rolled samples were water-cooled immediately after roll-bonding to minimize the structural change due to a heat generated by

*Corresponding author, E-mail: kamikawa@imr.tohoku.ac.jp

plastic deformation. The roll-bonded sheet was cut into half-length for the subsequent ARB process. The procedure of cutting, stacking and roll-bonding is referred to as 1 cycle of ARB and was repeated without changing the rolling direction through the process, up to 7 cycles for warm-temperature ARB at 400–600°C and 10 cycles for room-temperature ARB, corresponding to a total reduction of 99.2% and 99.9% or an equivalent strain of 5.6 and 8.0, respectively.

Microstructures of the ARB samples were characterized by electron backscatter diffraction (EBSD) in a scanning electron microscope (SEM) and transmission electron microscopy (TEM). Thin foils perpendicular to the transverse direction (TD), including the normal direction (ND) and rolling direction (RD) of the sheets, were prepared by electropolishing in a 100 ml $HClO_4$ + 900 ml CH_3COOH solution at 12°C and at a voltage of 20 V. EBSD measurements were carried out in an FEI XL30S SEM with a field emission gun operated at 20 kV using a program TSL OIM Data Correction, and obtained data were analyzed by a program TSL OIM Analysis. A Hitachi H-800 operated at 200 kV was used for the TEM observation.

3. Results

In the present study, a well-lubricated rolling has been used for the room-temperature ARB, and a non-lubricated rolling has been applied for the warm-temperature ARB at 400–600°C. The well-lubricated ARB is considered to introduce a relatively homogeneous rolling deformation through the sheet thickness, while the non-lubricated condition may cause a significantly inhomogeneous strain distribution throughout thickness due to a frictional shear deformation near the surface, so-called redundant shear deformation.[18–20] It can be considered that parabolic-shaped shear strain is introduced through the sheet thickness in a single ARB cycle, as shown in Fig. 1(a), where t_0 is the total thickness of the sample and t is the distance from the mid-thickness. Assuming that the same shear strain distribution is introduced in each ARB cycle, a schematic of the expected shear strain distribution after different ARB cycles can be obtained in Fig. 1(b)–(d). This clearly shows that the shear strain distribution becomes more complicated with increasing the number of ARB cycles, which may strongly affect the microstructure evolution during the processing. This effect has to be taken into account to compare the results between the room-temperature ARB and the warm-temperature ARB in this study.

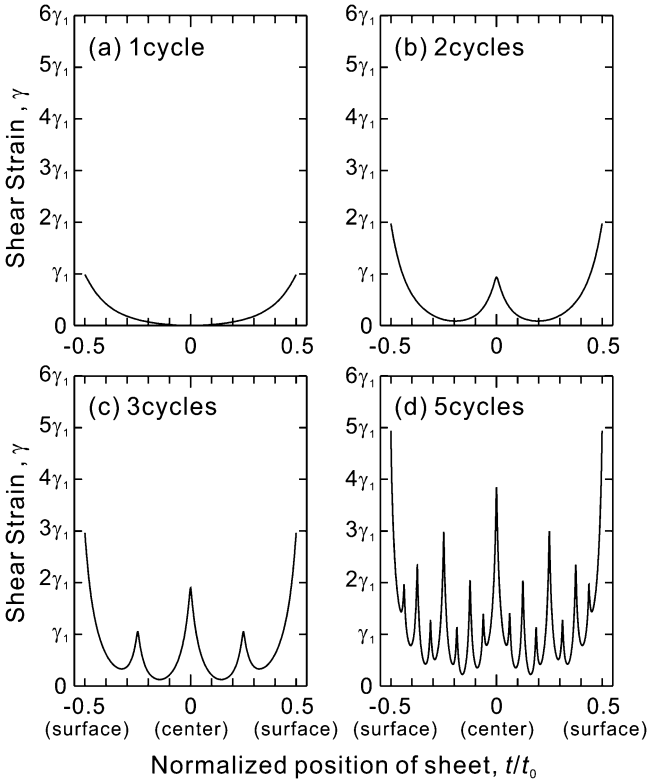

Fig. 1 Expected shear strain distribution in samples ARB processed without lubrication.

3.1 Room-temperature ARB

Microstructure evolution during the room-temperature ARB has been investigated using EBSD and TEM. Figure 2 shows grain boundary maps obtained by the EBSD measurements and TEM images for the samples deformed to different ARB cycles. Assuming that a homogeneous deformation is introduced in the well-lubricated room-temperature ARB, the EBSD images have been taken from the thickness-center layers. Green and red lines in the EBSD maps indicate boundaries with the misorientation angles above 15° and between 2–15°, respectively, and boundaries below 2° are cut off from the analysis in order to remove the error in the determination of such low-angle boundaries in EBSD. The fraction of high-angle boundaries (f_{HAGB}) determined by EBSD is indicated in the figure. The average boundary spacing has been measured from the TEM images, by linear intercept method along ND, referred to as boundary thickness (d_t), and is also indicated in the figure. In the 1-cycle ARB sample (Fig. 2(a)), most of the boundaries existing in the area are low-angle boundaries, although some initial grain boundaries with the high-angle misorientation are observed. The fraction of high-angle boundaries in this sample is around 10%. The TEM image of the 1-cycle sample shows a deformation cell structure with cell boundaries not parallel to RD, which is a typical deformation microstructure after low strain. The structure is more and more divided by deformation-induced high-angle boundaries, the fraction of which increases with increasing the strain, and such boundaries become more parallel to RD (Fig. 2(b)). After 5 cycles and above (Fig. 2(c), 2(d)), however, an ultrafine lamellar structure nearly aligned to RD is formed uniformly in the samples. The lamellar boundary spacing gradually decreases with increasing the strain, and it reaches to 88 nm in the 10-cycle ARB (Fig. 3). After 10 cycle ARB, the fraction of high-angle boundaries reaches up to approximately 80%. It should be noted that local shear bands have often been observed after 7 cycles and above, as indicated by arrows (Fig. 2(d)), and the occurrence of such shear deformation is more significant at higher strain. Localized shear deformation may be enhanced at high strain, since homogeneous deformation by dislocation slip within the hard matrix of ultrafine lamellae becomes difficult to occur at low temperature. An extreme case of shear localization

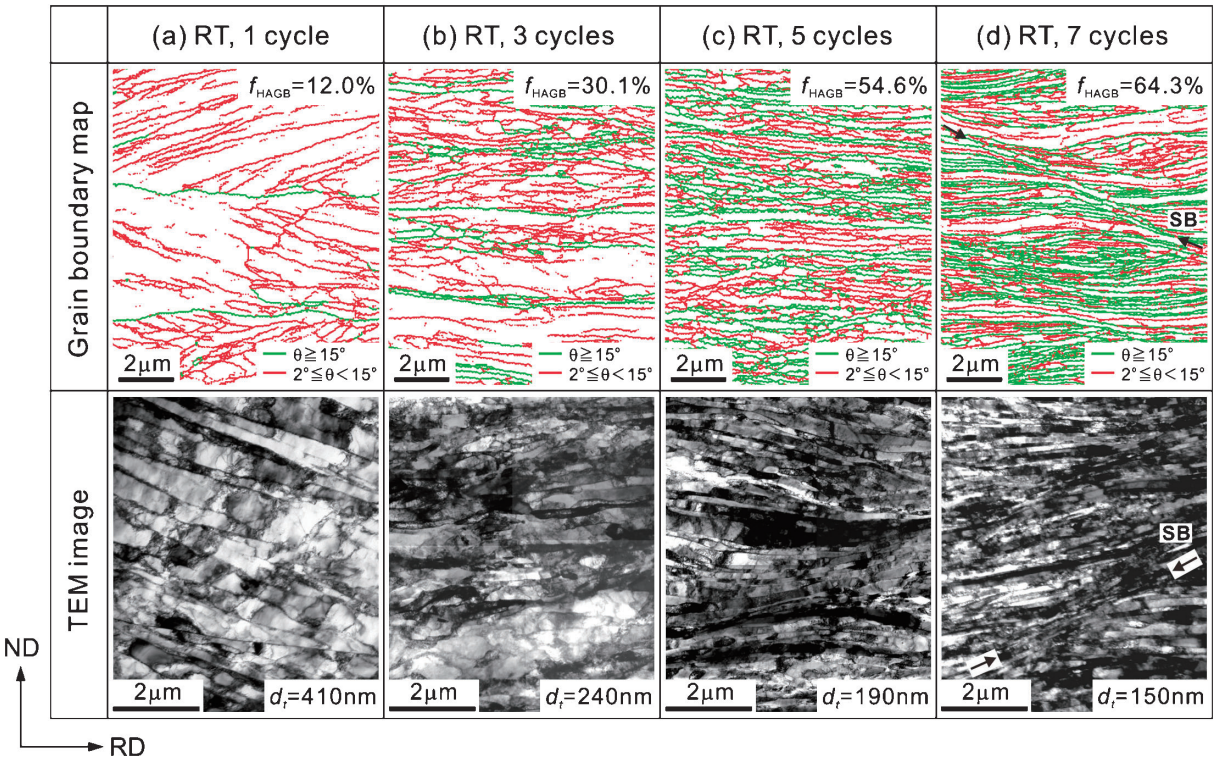

Fig. 2 Grain boundary maps and TEM images of the samples ARB processed by (a) 1 cycle, (b) 3 cycles, (c) 5 cycles and (d) 7 cycles at room temperature with lubrication.

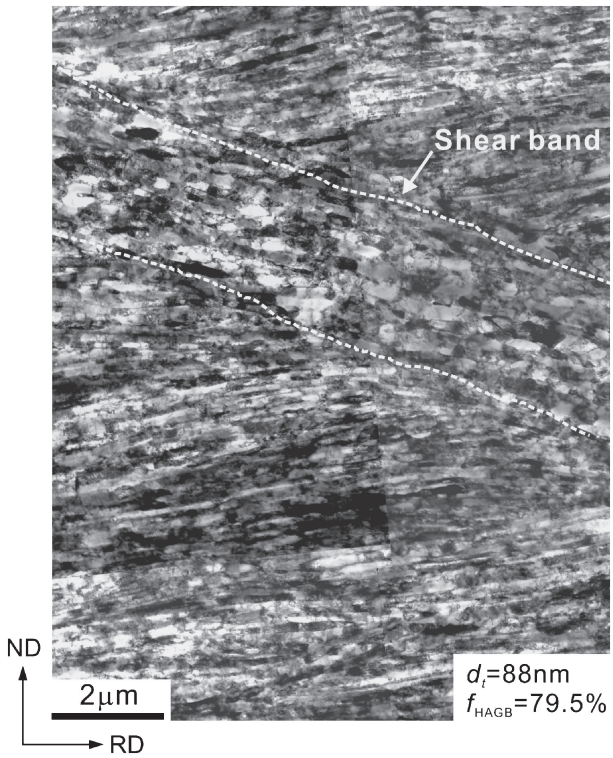

Fig. 3 TEM microstructure of the sample ARB processed by 10 cycles at room temperature with lubrication.

is observed in the 10-cycle ARB sample (Fig. 3), where a macroscopic shear band with a width of approximately 3 μm is dividing a matrix of lamellar boundary structure at an angle of approximately 30° with respect to RD. The structure within this localized shear band is more equiaxed than that in the lamellar boundary structure, resulting in a quite heterogeneous microstructure. The average spacing of the equiaxed structure within the shear band is measured as 260 nm, which is much larger than that of the matrix of lamellar boundary structure (88 nm). This difference must be due to a significant heat generation by the localized shear deformation, which is related to a large amount of strain and high strain rate deformation within the shear bands.

3.2 Warm-temperature ARB

Microstructural characterization by EBSD and TEM was carried out also for the samples ARB processed at warm-temperatures of 400–600°C without lubrication. In the case of non-lubricated ARB, the microstructural distribution is expected to be quite inhomogeneous due to the complicated redundant shear strain distribution, depending on both the number of ARB cycles and the thickness position of the sheets (see Fig. 1). Detailed microstructure evolution through the thickness during the non-lubricated 500°C ARB has previously been demonstrated by EBSD-based analysis,[19] and in this paper the EBSD maps from the thickness position of $t/t_0 \sim 0.1$ are only shown in Fig. 4. This position has been chosen to minimize the effect of redundant shear strain, since the total amount of shear strain in this layer is relatively small at least in the first few cycles, as can be seen in Fig. 1(a)–(c).

Figure 4 shows the grain boundary maps from EBSD and TEM micrographs of the samples ARB processed at 500°C by different cycles. These results have previously been reported elsewhere.[19,21,22] The 1-cycle ARB sample (Fig. 4(a)) shows a dislocation cell structure mainly composed of low-angle boundaries, similar to the sample

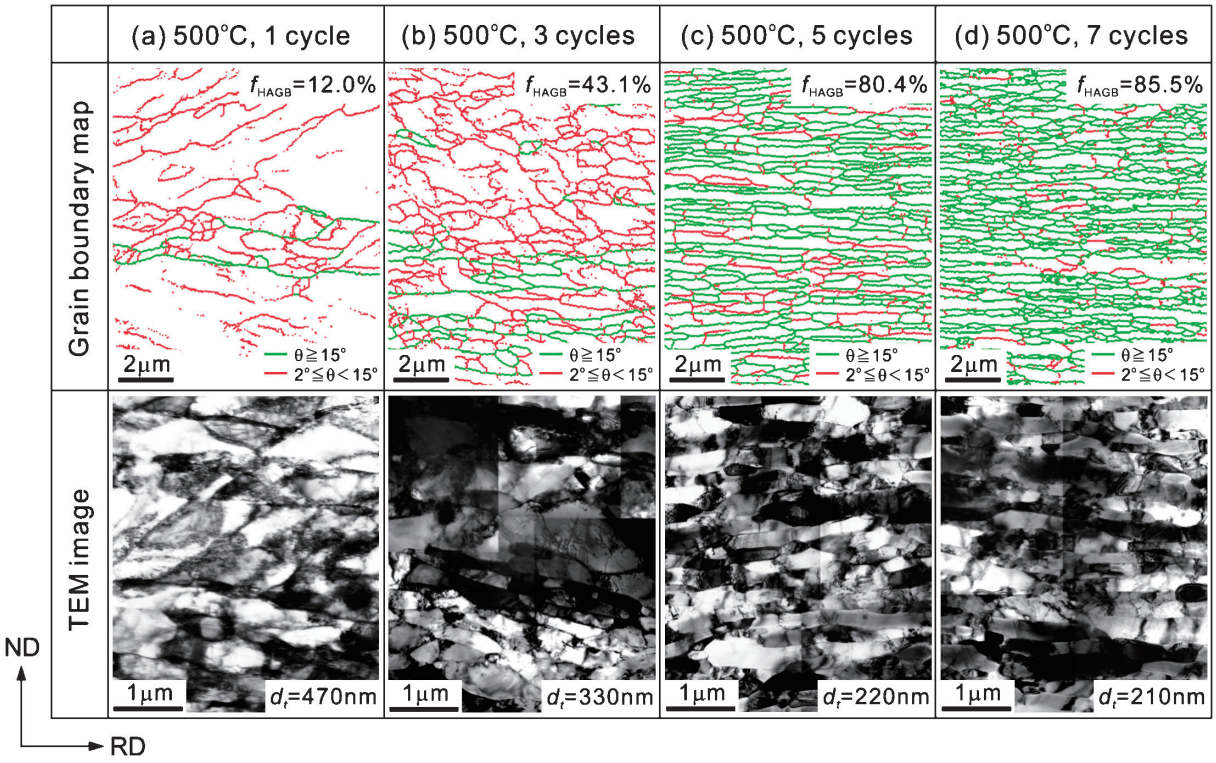

Fig. 4 Grain boundary maps and TEM images of the samples ARB processed by (a) 1 cycle, (b) 3 cycles, (c) 5 cycles and (d) 7 cycles at 500°C without lubrication.[19,21,22)]

deformed at room temperature (Fig. 2(a)). However, the cell boundaries are much wavy rather than straight, compared with the room-temperature ARB sample, indicating that cross slips of dislocations during the deformation have been enhanced at the higher deformation temperature. The fraction of high-angle boundaries increases and the average boundary thickness decreases with increasing the ARB cycle, and the 5-cycle ARB sample reveals a quite homogeneous structure subdivided by mostly high-angle boundaries with the average boundary spacing of 220 nm. The fraction of high-angle boundaries for this sample is 80.4%, much larger than that in the room-temperature ARB (54.6%, Fig. 2(c)), indicating that the formation of deformation-induced high-angle boundaries is accelerated by the non-lubricated ARB. It is seen from the EBSD and TEM images (Fig. 4(c)) that the structure after 5 cycles of ARB is elongated to RD but relatively equiaxed. This could be owing to an indication of enhanced recovery or boundary migration caused by elevated temperature deformation. Previous works[19,22)] have reported that the microstructures after the first few cycles of ARB were still heterogeneous through the thickness, affected by the redundant shear strain, but 5 cycles or more of ARB led to a quite homogeneous structure throughout the sample thickness. It should be emphasized here that the structures of the 5-cycle and 7-cycle samples are quite similar in terms of both boundary spacing and fraction of high-angle boundaries, indicating that the deformation structure tends to be saturated at high strain.

Structural observation using EBSD and TEM has been done for the samples deformed at 400°C and 600°C as well, and a similar microstructure evolution has been observed. Namely, the structure was being divided by deformation-induced boundaries and the boundary spacing decreased with increasing the ARB cycles, and an elongated ultrafine grained structure containing a large fraction of high-angle boundaries was homogeneously developed after 5 cycles of ARB, followed by a structural saturation after high strain. Figures 5(a) and 5(b) are the TEM microstructures after 7-cycle ARB at 400°C and 600°C, respectively. Quite uniform elongated structures are observed in both cases, similar to that for the 500°C ARB sample shown in Fig. 4(d), but the average boundary spacing becomes smaller with decreasing the deformation temperature. No significant shear band was observed in the warm-temperature ARB samples, indicating that the ultrafine grained structure can uniformly be deformed even at high strain at elevated temperatures. It has been confirmed from the EBSD measurements that these samples are subdivided mainly by high-angle boundaries, where the fraction of high-angle boundaries is approximately 80%, which is similar to those obtained after high strain in the room-temperature ARB or 500°C ARB.

3.3 Grain boundary spacing

Figure 6 summarizes the average boundary spacing along ND (d_t), determined from TEM microstructures, as a function of the equivalent rolling strain, ε_r, which can be determined as

$$\varepsilon_r = \frac{2}{\sqrt{3}} \ln \frac{1}{1-r} \quad (1)$$

where r is the total thickness reduction. The boundary spacing geometrically expected from the distortion of original grain boundaries ($d_{t,cal}$) is indicated as a broken line in the figure, which is given as,

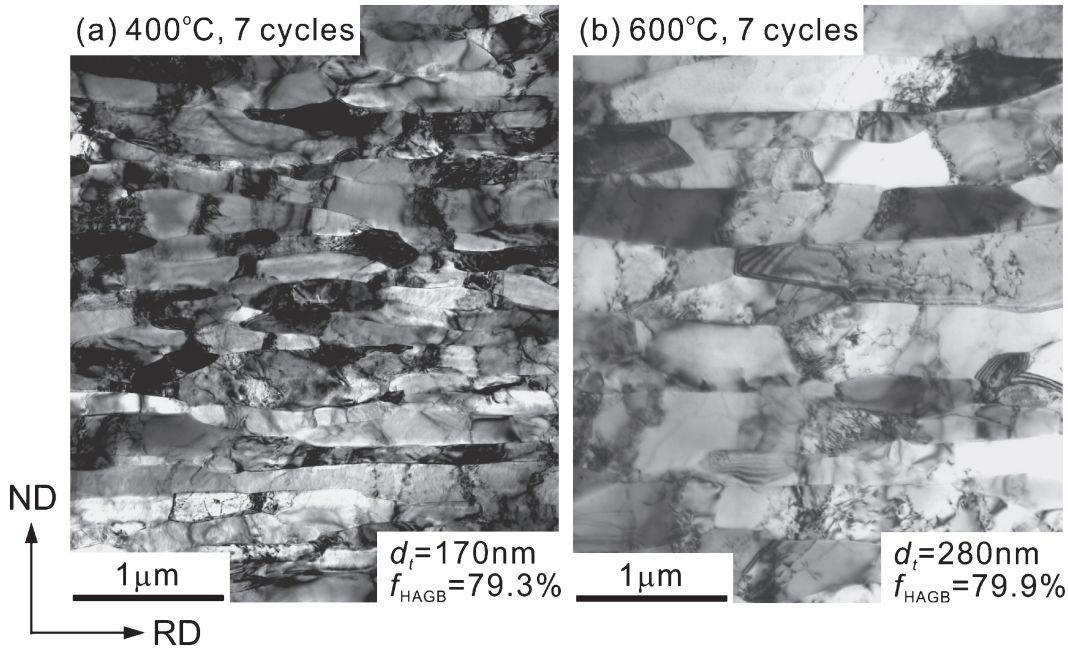

Fig. 5 TEM microstructures of the samples ARB processed by 7 cycles at (a) 400°C and (b) 600°C without lubrication.

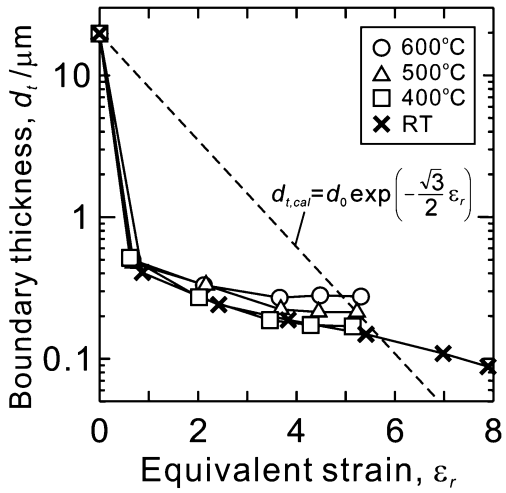

Fig. 6 Average boundary thickness (d_t) in the samples ARB processed at various temperatures.

$$d_{t,cal} = d_0 \cdot (1 - r) = d_0 \exp\left(-\frac{\sqrt{3}}{2}\varepsilon_r\right) \quad (2)$$

where d_0 is the initial grain size (= 20 μm). After 1 cycle of ARB, the average boundary spacing is below 1 μm at all deformation temperatures, which is much smaller than expected from a geometrical change in the initial grain boundaries ($d_{t,cal}$ = 10 μm after 1 ARB cycle, i.e. at an equivalent strain of 0.8), and the spacing decreases with increasing the strain. This result indicates that the original coarse grains have been subdivided by deformation-induced boundaries newly introduced by plastic deformation. In the early stage of deformation, such deformation-induced boundaries are low-angle ones, which are typically dislocation cell boundaries, as was shown in Figs. 2 and 4, but misorientation angles of the boundaries have become larger with increasing the strain. After a certain amount of strain, approximately a strain of 4, the microstructures are uniformly subdivided mainly by high-angle boundaries (see Fig. 4(c)–(d)). This formation mechanism of nanostructures during high strain deformation has been termed as *grain subdivision* by deformation-induced high-angle boundaries.[10,11] It should however be noted that the boundary spacing becomes saturated at the deformation temperature of 400°C and above, and tends to be even larger than the expected spacing of initial grain boundaries (the broken line), as is shown in Fig. 6. These observations suggest that the nanostructure formation by plastic deformation is not only controlled by grain subdivision, but also by other restoration mechanisms during the processing such as recovery and boundary migration. Possible mechanisms will be discussed in the next section.

4. Discussion

4.1 Structural saturation

The saturation of boundary spacing observed for the warm-temperature ARB samples is quite interesting because the boundary spacing is expected to be half in each ARB cycle from the geometrical shape change. Note here that in the warm-temperature ARB the stacked sheets have been kept in an air furnace at elevated temperature for 10 min before the roll-bonding. Therefore, some static recovery or boundary migration may occur during this re-heating treatment. In order to know the structural change during the re-heating, the 5-cycle samples in the warm-temperature ARB were heated for 10 min at each elevated temperature and immediately water-cooled without the roll-bonding process. The microstructures of these samples were observed by TEM. By the boundary spacing measurement for TEM images, the boundary spacing (d_t) after 10-min heating was determined to 210 nm, 310 nm and 400 nm in the 400°C, 500°C and 600°C ARB, respectively. The boundary spacing

after re-heating is smaller than double the spacing of 5-cycle sample in each temperature. It has therefore been confirmed that the microstructural coarsening during the re-heating is not so significant, and such effect can be ignored.

One may argue that another possibility of the structural saturation is due to grain boundary sliding during the rolling deformation. However, it can also be ruled out because of a high strain-rate deformation ($\sim$19 s^{-1}) in the present roll-bonding at a relatively low-temperature deformation (0.37–0.48 T_m; T_m is the melting point in Kelvin) and an elongated structural morphology, which would make the accommodation process necessary for grain boundary sliding quite difficult.

It can therefore be assumed that the main structural coarsening responsible for the structural saturation is taking place dynamically during the deformation. More detailed discussion is described in the next section.

4.2 Zener–Hollomon parameter dependence

Based on the above discussion, it can be considered that the structural saturation observed in this study mainly occurs during the deformation process, which is quite similar to the behavior of steady-state dynamic recrystallization or dynamic recovery during high-temperature deformation,[23–25] where the dynamically recrystallized grain size or subgrain size remains constant independent of applied strain at high strain stage. It is well known that an average grain size or subgrain size in the steady-state dynamic recrystallization or dynamic recovery can be explained as a function of Zener–Hollomon (Z) parameter expressed in a following equation,[25–27]

$$d = A \cdot Z^{-B} \tag{3}$$

where d is the grain size or subgrain size, A and B are the constants. The Z is the temperature-compensated strain rate and is described as,[23]

$$Z = \dot{\varepsilon} \exp \frac{Q}{RT} \tag{4}$$

where $\dot{\varepsilon}$ and T are the strain rate and temperature during the deformation, respectively. Q is the (apparent) activation energy for the high-temperature deformation and R (= 8.314 J mol^{-1} K^{-1}) is the gas constant. The eq. (3) indicates that the grain size or subgrain size obtained by dynamic recrystallization or recovery is smaller as the Z parameter is lower, in other words, the strain rate is higher or the deformation temperature is lower.

To understand the mechanism of the structural saturation, the lamellar boundary spacing (d_t) obtained at high strain is plotted as a function of Z parameter in Fig. 7. The lamellar boundary spacing after 7 cycles is used as the grain size in the warm-temperature ARB, where the spacing tends to be saturated. The data for 10-cycle room-temperature ARB is also plotted even though the spacing is not saturated yet. For Z estimation, several assumptions were considered as described below. The activation energy for self diffusion of iron atom (254 kJ mol^{-1}) was used for Q. The strain rate was calculated taking account of the roll flattening, and deformation temperatures were modified considering the temperature increase caused by the plastic work during the rolling. Data from previous works are also plotted in the

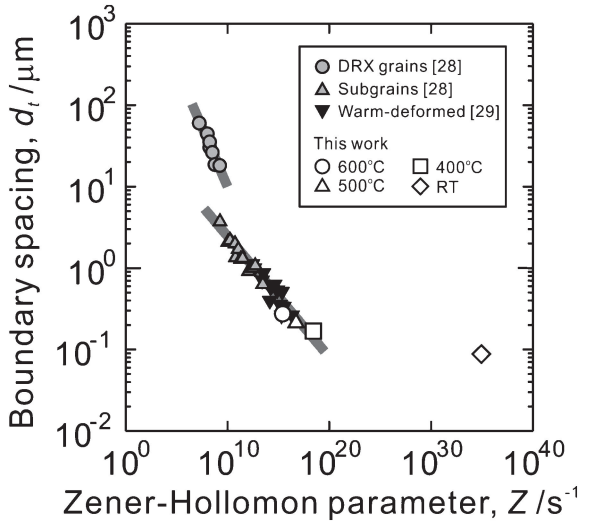

Fig. 7 Relationship between the average boundary spacing and Zener–Hollomon parameter in the samples deformed to high strains by ARB at different temperatures.

figure. The gray circles and triangles are the data from recrystallized grains and subgrains, respectively, in discontinuous dynamic recrystallization in a hot deformed IF steel.[28] The black triangles are from a low carbon steel severely warm deformed by plane strain compression,[29] in which significant boundary migration did not occur during the deformation.

The figure shows that the linear relationship of the DRX grains is located at a much larger grain size range than that of subgrain/warm-deformed samples. This is due to the fact that discontinuously recrystallized grains are accompanied with long-range migration of recrystallized grain boundaries, while in subgrained or warm-deformed structures dynamic recovery and short-range boundary migration would be dominant to determine the structural size. It is noted that three data points from warm-temperature ARB at 400–600°C in this work can be plotted on the extrapolation of the linear relationship from subgrains/warm-deformed samples, suggesting that a similar mechanism of microstructure evolution could be operating in this category, which is supported by the facts that no abnormally migrated grains (discontinuously recrystallized grains) has been observed in the warm-temperature ARB samples (Figs. 4 and 5). It can therefore be concluded that the formation of nanostructures by high strain deformation can be understood by a balance of grain subdivision and dynamic recovery or short-range boundary migration. It is also suggested that increasing the Zener–Hollomon parameter is effective to obtain a finer structural size.

On the other hand, the data point from the room-temperature ARB is not on the extrapolation of the curves from subgrained/warm-deformed samples. In the room-temperature ARB at high strain, the localized shear banding could be a more dominant mechanism for plastic deformation, and the matrix of lamellar boundary structure is not so much plastically deformed. In other words, in this condition, mechanisms of plastic deformation are different from those in the warm-temperature deformation, which could be the reason for a large deviation from the extrapolated curves.

4.3 Optimization of deformation temperature and strain rate

This study suggested that increasing Zener–Hollomon parameter, that is, decreasing the deformation temperature or increasing the strain rate, is effective to obtain a finer grain size in highly strained materials. This strategy could be true in general to suppress structural coarsening during the deformation. However, as demonstrated in this work, if the temperature is too low, e.g. room temperature in the present case, a localized shear deformation has macroscopically been introduced in the sample, leading to a mixed structure of ultrafine lamellae and local shear bands (see Fig. 3). Such a heterogeneous structure is however unwanted in general, since it may lead to heterogeneities in local mechanical properties and discontinuous recrystallization when annealed at elevated temperature. It is therefore suggested that a moderate deformation temperature, neither too high nor too low, has to be selected to avoid the occurrence of localized shear deformation.

In the present work, the deformation temperature has only varied, and the effect of strain rate has not been investigated in detail. However, it may be possible to see the effect of strain rate by the occurrence of local shear banding in the room-temperature ARB. It has been observed in Fig. 3 that the structure within the shear bands is much coarser than the matrix of lamellar boundary structure. These results can be understood in the following way. When local shear banding occurs, plastic deformation mainly concentrates on the sheared regions, resulting in a high strain rate deformation as well as a high amount of strain within the shear localized areas. Therefore, the work of plastic deformation becomes much larger in the shear bands than in the matrix. This leads to a large and adiabatic heat generation, so that dynamic recovery or boundary migration are more enhanced. In particular, since nanostructures are composed of narrowly spaced high-angle boundaries and many dislocations between the boundaries, which gives higher driving force for restoration reactions and may accelerate a diffusion process, the effect of heat generation on the structural coarsening cannot be neglected. The fact that increasing the strain rate rather produces a larger grain size has also been reported in a previous work on an ARB processed commercial purity aluminium,[30] which corresponds with the present results.

It can therefore be suggested from the above discussion that decreasing the deformation temperature or increasing the strain rate is not always an effective strategy to produce nanostructured metals by high strain deformation. Appropriate deformation conditions should be chosen to avoid the occurrence of localized shear banding and to produce homogeneous nanostructured metals with a uniform mechanical-property distribution and a good thermal stability.

5. Conclusions

The microstructure and mechanical properties of IF steel samples deformed by ARB at different temperatures in the range from room temperature to 600°C have been investigated. The results obtained are summarized as follows.

(1) In all temperature range, ultrafine lamellar boundary structures surrounded by high-angle boundaries are obtained after several numbers of ARB cycle. The grain refinement mechanism of such nanostructures can be understood as grain subdivision by plastic deformation where original coarse grains have been subdivided by deformation-induced boundaries into a nanoscale regime.

(2) The boundary spacing decreases with increasing the applied plastic strain, but it tends to be saturated at high strain. The saturated boundary spacing is smaller as the deformation temperature is lower, and the saturated boundary spacing can be explained as a function of Zener–Hollomon parameter. It is suggested that nanostructures by plastic deformation are formed by a balance of grain subdivision and restoration by recovery or short-range boundary migration during the deformation, and that lowering the deformation temperature is effective to reduce the structural size.

(3) Localized shear banding becomes dominant for plastic deformation of the nanostructures at room temperature, leading to heterogeneities in the microstructure. It is therefore suggested that a moderate deformation temperature as well as strain rate should be required to produce nanostructured metals with a homogeneous structural distribution.

Acknowledgement

This study was financially supported by the Grant-in-Aid for Scientific Research on Innovative Area, “Bulk Nanostructured Metals”, through MEXT, Japan (contract No. 22102006), which is gratefully appreciated.

REFERENCES

1) M. A. Meyers, A. Mishra and D. J. Benson: Prog. Mater. Sci. **51** (2006) 427–556.
2) N. Tsuji, Y. Ito, Y. Saito and Y. Minamino: Scr. Mater. **47** (2002) 893–899.
3) Y. Wang, M. Chen, F. Zhou and E. Ma: Nature **419** (2002) 912–915.
4) Y. Kimura, T. Inoue, F. Yin and K. Tsuzaki: Science **320** (2008) 1057–1060.
5) N. Kamikawa, X. Huang, N. Tsuji and N. Hansen: Acta Mater. **57** (2009) 4198–4208.
6) L. L. Shaw: J. Metals (JOM) **52** (2000) 41–45.
7) M. J. Zehetbauer and Y. T. Zhu: *Bulk Nanostructured Materials*, (Wiley-VCH, Weinheim, 2009).
8) B. S. Altan (editor): *Severe Plastic Deformation: Toward Bulk Production of Nanostructured Materials*, (NOVA Science Publishers, New York, 2006).
9) R. Z. Valiev, R. K. Islamgaliev and I. V. Alexandrov: Prog. Mater. Sci. **45** (2000) 103–189.
10) Q. Liu and N. Hansen: Proc. R. Soc. London A **454** (1998) 2555–2591.
11) N. Hansen and D. Juul Jensen: Phil. Trans. R. Soc. London A **357** (1999) 1447–1469.
12) A. Gholinia, F. J. Humphreys and P. B. Prangnell: Acta Mater. **50** (2002) 4461–4476.
13) H. Jazaeri and F. J. Humphreys: Acta Mater. **52** (2004) 3239–3250.
14) N. Tsuji, N. Kamikawa and B. Li: Mater. Sci. Forum **539–543** (2007) 2837–2842.
15) A. Vorhauer and R. Pippan: Metall. Mater. Trans. A **39A** (2008) 417–429.
16) Y. Saito, H. Utsunomiya, N. Tsuji and T. Sakai: Acta Mater. **47** (1999) 579–583.
17) N. Tsuji, Y. Saito, S. H. Lee and Y. Minamino: Adv. Eng. Mater. **5** (2003) 338–344.

18) S. H. Lee, Y. Saito, N. Tsuji, H. Utsunomiya and T. Sakai: Scr. Mater. **46** (2002) 281–285.
19) N. Kamikawa, T. Sakai and N. Tsuji: Acta Mater. **55** (2007) 5873–5888.
20) W. F. Hosford and R. M. Caddell: *Metal forming*, (PTR Prentice Hall, 1993).
21) N. Kamikawa, N. Tsuj and Y. Saito: Tetsu-to-Hagane **89** (2003) 273–280 (in Japanese).
22) N. Kamikawa, N. Tsuji and Y. Minamino: Sci. Tech. Adv. Mater. **5** (2004) 163–172.
23) F. J. Humphreys and M. Hatherly: *Recrystallization and Related Annealing Phenomena*, Second Edition, (Elsevier, UK, 2004).
24) C. M. Sellars: Proc. 7th Risø Int. Symp. on Metallurgy and Materials Science, (1986) pp. 167–187.
25) B. Derby: Acta Metall. Mater. **39** (1991) 955–962.
26) T. Maki, K. Akasaka and I. Tamura: Proc. Int. Conf. on the Thermomechanical Processing of Microalloyed Austenite, (1981) pp. 217–236.
27) T. Maki, K. Akasaka, K. Okuno and I. Tamura: Tetsu-to-Hagane **66** (1980) 1659–1668 (in Japanese).
28) N. Tsuji, Y. Matsubara, Y. Saito and T. Maki: J. Japan Inst. Metals **62** (1998) 967–976 (in Japanese).
29) A. Ohmori, S. Torizuka, K. Nagai, N. Koseki and Y. Kogo: Mater. Trans. **45** (2004) 2224–2231.
30) N. Tsuji, T. Toyoda, Y. Minamino, Y. Koizumi, T. Yamane, M. Komatsu and M. Kiritani: Mater. Sci. Eng. A **350** (2003) 108–116.